Tephra-Fall Deposits from the 1992 Eruptions of Crater Peak, Mount Spurr Volcano, Alaska: A Preliminary Report on Distribution, Stratigraphy, and Composition

By Christina A. Neal, Robert G. McGimsey, Cynthia A. Gardner, Michelle L. Harbin, and Christopher J. Nye

CONTENTS

ABSTRACT

Most ejecta from the 1992 eruptions of Crater Peak was deposited as tephra fall from eruption columns that ascended rapidly to altitudes of greater than 14 km above sea level, Coarse bomb- to fine ash-sized tephra fell along relatively narrow trajectories extending north, northeast, and east from the vent; these patterns reflect prevailing wind directions in upper Cook Inlet. Each brief (3.5- to 4.0-hour), small-volume (12 to 15 x 106 m^3 dense rock equivalent or DRE) eruption involved two distinct juvenile andesitic tephra components that differ in color and density only; no systematic differences in glass chemistry, bulk composition, or mineralogy have been identified. The stratigraphic relations of these components in the August 18 and September 16–17 deposits suggest that the upper part of an inferred pre-eruption magma body was enriched in volatiles relative to the lower part. Clast-size grading may reflect a progressive increase in magma discharge during the first 2 to 3 hours of tephra emission.

INTRODUCTION

After 39 years of quiescence, the Crater Peak vent on the south flank of Mount Spurr volcano reawakened with a series of three short lived but violent eruptions of andesitic tephra on June 27, August 18, and September 16–17 of 1992 (Eichelberger and others, this volume; Alaska Volcano Observatory, 1993). Each eruption lasted 3.5 to 4.0 hours and generated vulcanian to subplinian eruption columns that reached altitudes of more than 14 km above sea level (ASL). Carried downwind, these tephra plumes resulted in narrowly distributed fall deposits composed principally of poorly vesiculated, crystal-rich juvenile andesite that ranged in size from coarse bombs to fine ash. Plumes from the three eruptions extended north, northeast, and east away from the volcano. Two of the three 1992 events deposited significant amounts of fallout tephra onto the most heavily populated areas of south-central Alaska (fig. 1A).

Tephra-fall deposits make up the bulk of the eruptive volume for each event (12, 14, 15 x 10^6 m^3 DRE for the three eruptions) and hence contain critical information regarding temporal changes in chemistry, eruption dynamics, and plume behavior. Each eruption also produced small pyroclastic flows and lahars, however, together these deposits make up less than I percent of the total bulk volume for the entire eruption series (Miller and others, this volume; D. Meyer, oral commun., 1994). This paper summarizes field characteristics and preliminary compositional analyses of proximal tephra-fall deposits, and it also proposes a model to explain observed physical and sedimentologic variations.

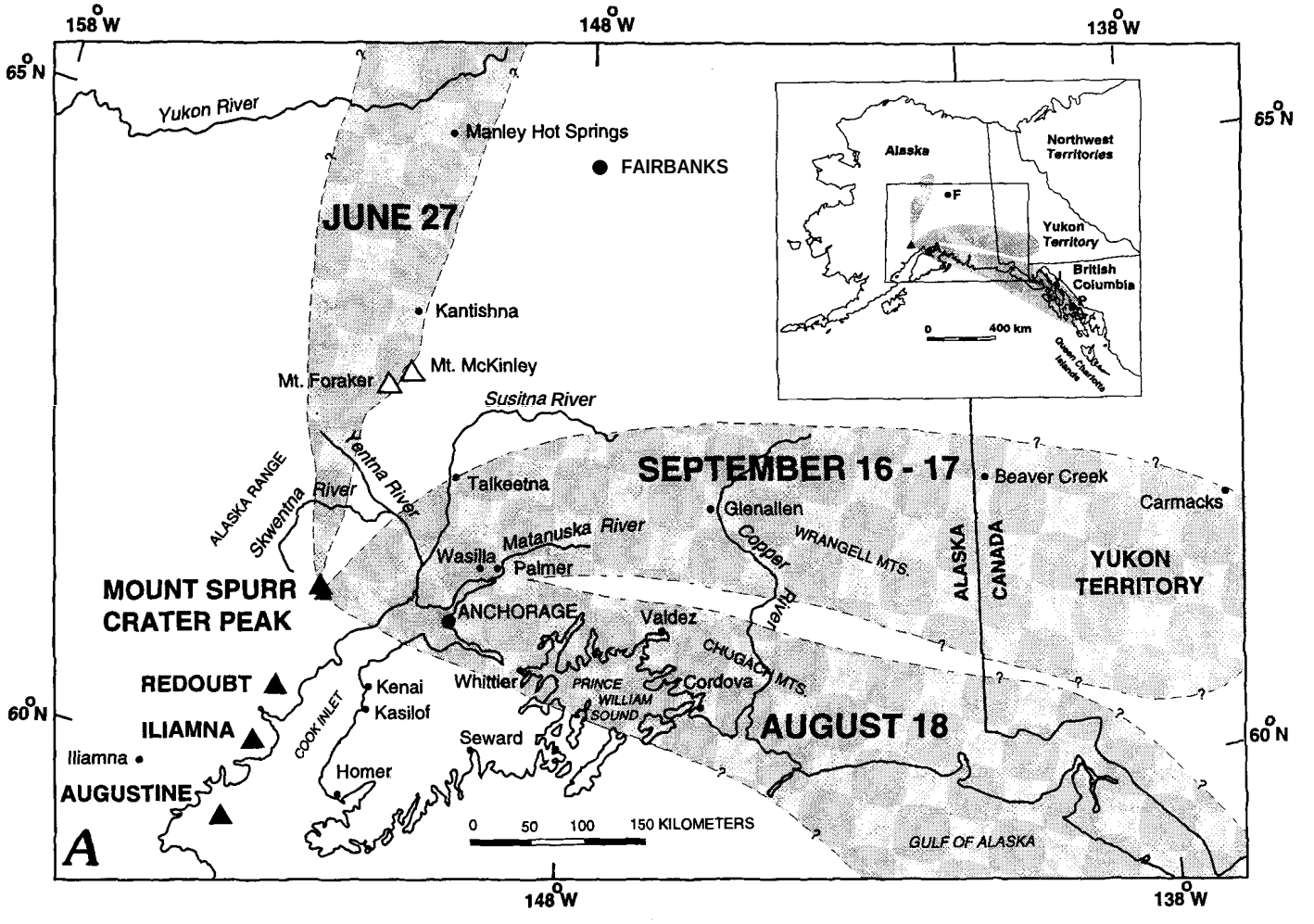

Figure 1. *A*, Generalized map showing extent of the three tephra-fall deposits from the 1992 eruptions of Crater Peak, Mount Spurr volcano, Alaska. Shaded areas denote approximate limits of tephra-fall inferred from ground and aerial surveys within 250 km of the vent as well as phone contact with distant communities within several days of the eruptions. Due to very sparse population and poor road access, the actual downwind extent of each deposit is unknown.

ACKNOWLEDGMENTS

The 1992 Mount Spurr eruption response was a team effort and we thank the entire AVO staff and many AVO affiliates for their contributions to this study. Tom Miller and Jim Begét shared observations of the June 27 deposits. Terry Keith, Deb McGimsey, and Judith Radwany assisted in sampling. Marvin Couchman is gratefully acknowledged for his measurements of clast densities. Lee Kelley of the National Weather Service (NWS) provided information on radar observations. We would also like to thank members of the public, other U.S. government agencies, Transport Canada, and the Canadian Geological Survey for sharing important observations of the eruption plume and tephra fall. Kathy Lemke and Ann Vanderpool assisted with computer graphics. Reviews by Steve Self, Richard Waitt, and Steve Carey significantly improved the content and presentation of this paper.

DISTRIBUTION OF TEPHRA-FALL DEPOSITS

Prevailing winds in upper Cook Inlet (fig. 1*B*) blow from the southeast, southwest, and northwest; the dominant wind direction is from the south to southwest. Consequently, tephra erupted from any Cook Inlet volcano is likely to be carried over populated areas and into the busy air traffic corridor of south-central Alaska; this phenomenon underscores the need for timely eruption notification and tracking of tephra plumes. As part of eruption-response procedures at the Alaska Volcano Observatory (AVO), hypothetical plume trajectory plots provided by the NWS were generated at AVO (Brantley, 1990, fig. 32). Based on twice-daily atmospheric soundings of wind velocity at various altitudes, these maps are used to forecast probable dispersal patterns of tephra plumes and resultant fallout

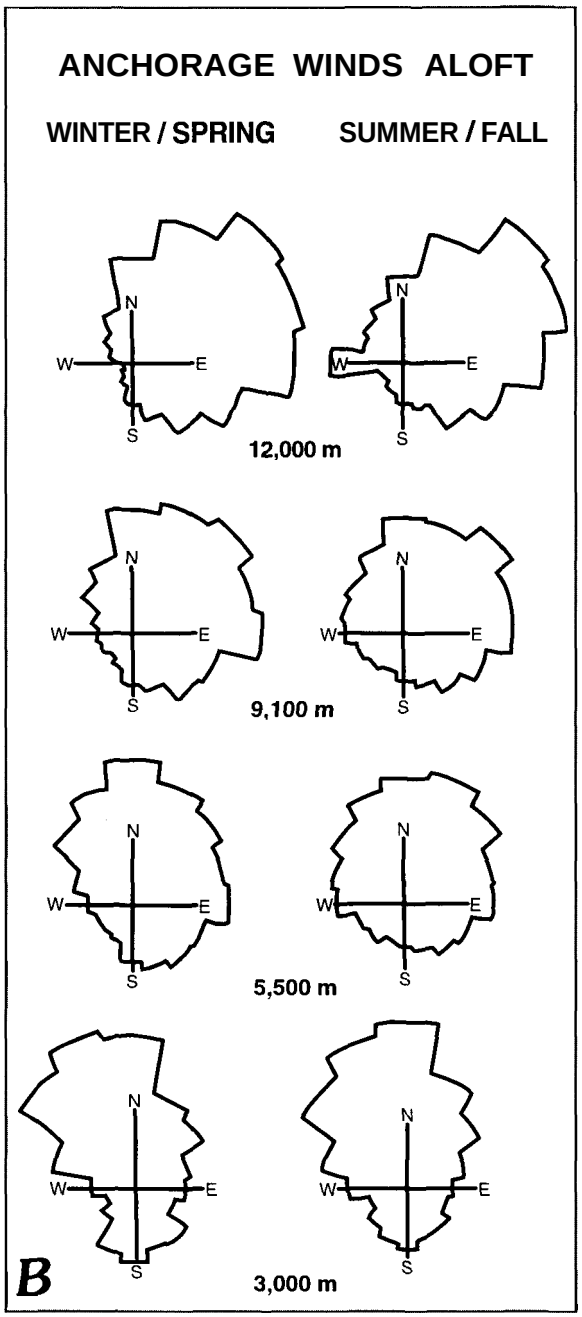

Figure 1. Continued. B, Compass rose diagrams indicate percent of time that winds blow toward a given direction over Anchorage (adapted from Till and others, 1993, and based on data from the National Climatic Data Center, Asheville, North Carolina for the period 1948 to 1972).

(Murray and others, 1994). All three tephra plumes produced during the 1992 eruptions at Crater Peak followed trajectories in good agreement with these plots.

The June 27 eruption occurred during a period of strong southerly winds and heavy overcast. As determined by C-band (5.4-cm-wavelength) radar operated by NWS, the vertical eruption column reached a maximum altitude of 14.5 km ASL by 10:23 a.m. Alaska Daylight Time (ADT), approximately 3.3 hours into the eruption (Rose and others, this volume). The tephra plume traveled north from Crater Peak (fig. 1*A*) over the relatively unpopulated Yentna and Skwentna River basins, the Alaska Range near Mount Foraker, and the settlement of Kantishna. The most distal report of ash fall was received from Manley Hot Springs, 140 km west of Fairbanks and 420 km north of Crater Peak. To the north of this community, there are few settlements.

During the August 18 eruption, winds were westerly and the axis of the main tephra fall extended east from Crater Peak, across Cook Inlet and over the Anchorage basin where 1 to 3 mm of primarily coarse ash was deposited. The plume continued southeastward over Prince William Sound, the eastern Chugach Mountains, and the Gulf of Alaska (fig. 1*A*). Petersburg, Alaska, 1,200 km southeast of Crater Peak (fig. 1*A*, inset) reported a light dusting of fine ash on August 19. Farther south, in the Queen Charlotte Islands and along coastal British Columbia, Canadian Flight Service Station personnel noted only the passage of a hazy layer overhead. In distribution, this fallout pattern is similar to that of the 1953 Crater Peak eruption; tephra accumulation in Anchorage, however, was greater in 1953 (3–6 mm; Wilcox, 1959). The maximum radar-discernible plume height during the August 18, 1992, eruption was 13.7 km ASL at 4:55 p.m. ADT (Rose and others, this volume), only 14 minutes after the onset of the main phase of the eruption. Pilot estimates of the top of the visible plume suggested actual heights may have been in excess of 18 km.

The September 16–17 eruption occurred during southwesterly winds and the plume traveled northeast over the communities of Wasilla and Palmer in the Matanuska-Susitna valley, parts of the Talkeetna Mountains, the Copper River Basin, and east into the Yukon Territory of Canada (fig. 1*A*). The farthest reported ash fall was in Carmacks, Yukon Territory, 860 km from Crater Peak. Light and variable low-level winds on September 16 and 17 accounted for numerous reports of very light dustings of ash as far south as Anchorage. Maximum radar-discernible plume height was 13.9 km ASL by 2:21 a.m. ADT, September 17 (Rose and others, this volume), more than 2 hours after the eruption began. Because the eruption occurred at night, there were few pilot reports of column height to corroborate this estimate.

VOLUME OF TEPHRA-FALL DEPOSITS

Helicopter-supported mapping and road access to large areas affected by the August 18 and September 16–17 eruptions allowed for rapid measurement of tephra-fall deposit thicknesses within south-central Alaska. Most data and samples were gathered within several days to 1 week of the eruption. With the exception of some wetting and compaction owing to rainfall or incorporation of water from melting snow and ice substrate, no significant reworking of the deposits was evident during collection of most samples. For each of the three tephra-fall deposits, we collected between 5 and 50 measured area samples (typically 20 x 20 cm) along and across the deposit axis as far as 190 km from Crater Peak. Based on mass per unit area data (Scott and McGimsey, 1994; Fierstein and Nathenson, 1992), the DRE volumes (using 2,600 kg/m^3) calculated for each event are 12 x 10^6 m^3, 14 x 10^6 m3, and 15 x 10^6 m^3 for the June 27, August 18, and September 16–17 eruptions, respectively. Bulk volumes calculated using the same method and a density of 700 kg/m^3 are 44 x 10^6 m^3, 52 x 10^6 m3, and 56 x 10^6 m3.

THICKNESS OF TEPHRA-FALL DEPOSITS

Stable wind conditions during each brief eruption contributed to fairly uniform changes in thickness and grain size with increasing distance from the vent. Proximal tephra-fall deposits for each eruption range similarly in thickness from about 1 m at the base of Crater Peak (approximately 1 km from vent) to 10 cm at a 10-km distance (fig. 2). At a distance of 100 km, the total ash fall is only a few millimeters thick. Over the same distance, modal grain size varies roughly from cobble gravel near the vent to coarse sand at 100 km. Additional grain-size analyses are in progress to further characterize the deposits.

COMPOSITION OF TEPHRA-FALL DEPOSITS

Most tephra from each eruption consists of juvenile andesite fragments of two distinct colors, tan and gray. For the August 18 and September 16–17 tephra sequences, lower and upper stratigraphic units (layers A and B, respectively) reflect a distinct change in the proportion of the two colors (table 1). Overall, the deposits are volumetrically dominated by tan to light-brown, slightly pumiceous, angular, equant to pyramidal fragments of crystal-rich andesite. Many clasts were fractured during ejection or deposition and have one or more flat or slightly concave faces. Lapilli (1–3 cm) commonly show gradational color variations from tan exteriors to dark-brown interiors. Inclusions of vesiculated basement clasts; dense gray, aphyric volcanic lithics; and rounded, sugar-textured, plagioclase-pyroxene crystal clots are common and are similar to inclusions found in the breadcrusted bombs of the pyroclastic-flow deposits (Miller and others, this volume; Nye and others, this volume; Harbin and others, this volume). Second in abundance are light- to medium-gray, microvesicular, crystal-rich andesite clasts that predominate in the upper part of the August 18 and September 16–17 tephra sections. These clasts are smaller in grain size and denser (table 2) than accompanying tan clasts, but they contain similar lithic, crystal-clot, and exotic pumiceous inclusions. They are angular to subrounded and generally equant in shape.

Accidental clasts make up a small volume of the tephra-fall deposits. These clasts consist of pre-1992 Crater Peak volcanic rocks recognized on the basis of alteration, fragments of coarse-grained metamorphic and possibly plutonic basement, crystal clots, and vesiculated clasts of basement rock (table 1; Harbin and others, this volume; Miller and others, this volume). A representative proximal sample of each tephra-fall unit was selected, and between 900 and 3,400 clasts were sorted and counted for each sample; percentages listed below and in table 1 represent the proportion of counted clasts. Fragments were classified on the basis of gross visual characteristics. Although these counts represent only a limited view of each deposit, we noted no field evidence of gross spatial changes in deposit character, and hence consider these percentages to be good first-order representations of each unit.

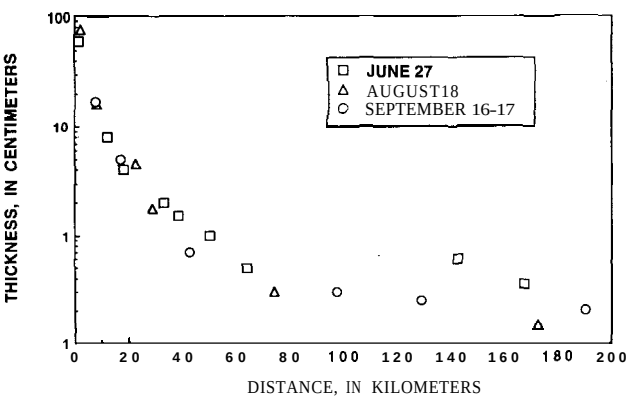

Figure 2. Thickness of tephra-fall deposits from the 1992 eruptions of Crater Peak, Mount Spurr volcano, Alaska, measured downwind along an approximate axis of each plume. The two most distant points for June 27 tephra were measured in the late summer of 1993 and are considered anomalously thick owing to percolation of the fine sand-sized tephra across a recrystallized snow layer.

Table 1. Percentage of clast types for tephra-fall deposits from the 1992 eruptions of Crater Peak, Mount Spurr volcano, Alaska.

[Populations determined by hand picking from size fraction larger than -1.75 phi (approximately 3 mm). Similar calculations based on weight or volume of each clast type produce nearly identical results. See text for description of each clast type.]

	Tan andesite	Gray andesite	Pre-1992 volcanics	Metamorphic and plutonic	Total clasts
June 27	78	14	7	1	1761
August 18 layer A	70	23	6	1	3355
August 18 layer B	6	91	3	0	1067
September 16–17 layer A	79	15	5	1	2630
September 16–17 layer B	26	64	10	0	918

Table 2. Densities, (in g/cm^3) for selected juvenile tephra clasts from the 1992 eruptions of Crater Peak, Mount Spurr volcano, Alaska.

[Note the similarity in component densities for August and September. Overall, June clasts of both types are 10 to 15 percent denser than clasts from the other two eruptions. Densities were measured by M. Couchman following techniques described in Hoblitt and Harmon (1993).]

June tan	June gray	August layer A tan	August layer A gray	August layer B tan	August layer B gray	September layer A tan	September layer A gray	September layer B tan	September layer B gray
1.98	2.21	1.59	1.98	1.65	1.98	1.61	1.85	1.54	1.83
1.56	2.08	1.52	2.07	1.57	1.98	1.60	1.75	1.65	1.93
1.76	1.91	1.93	1.86	1.32	1.85	1.37	1.89	1.53	1.92
1.86	1.98	1.47	2.47	1.69	2.14	1.69	2.02	1.80	2.70
1.78	2.14	1.67	2.07	1.55	1.80	1.86	1.87	1.73	1.99
1.92	2.38	1.69	1.87	1.48	2.04	1.76	1.59	1.14	2.09
1.66	2.03	1.34	1.89	1.48	2.46	1.16	1.73	1.64	2.05
1.44	1.93	1.40	1.88	1.55	2.02	1.53	1.47		
1.93	2.72	1.87	2.07	1.53	1.93	1.71	2.41		
1.82	2.04	1.43	1.96	1.29	1.81	1.62	2.38		
1.86	2.69	1.41	2.36	1.62	1.95	1.88	2.61		
1.58	2.76	1.48	1.97	1.58	2.56	0.98	2.71		
1.58	2.45	1.57	2.48	1.47	1.81	1.59	2.25		
1.91	2.67	1.51	2.09	1.43	2.03	1.76	1.85		
1.87	2.10	1.70	2.02	1.43	1.96	1.33	1.79		
2.01		1.67	1.97	1.41	1.89	1.62			
1.91		1.62	2.33	1.31	2.10	1.41			
1.79		1.38	1.88	1.61	1.90	1.33			
1.43		1.45	1.94	1.55	2.01	1.25			
1.49		1.38	1.86	1.55	2.01	1.51			
				Average densities					
1.76	**2.27**	**1.55**	**2.05**	**1.50**	**2.01**	**1.53**	**2.01**	**1.58**	**2.07**

STRATIGRAPHY OF TEPHRA-FALL DEPOSITS

JUNE 27

The June 27 tephra-fall deposit is light gray to tan in color, moderately well sorted, and shows weak reverse grading. Angular clasts of tan to light-brown, poorly vesicular, porphyritic juvenile andesite are the dominant component (78 percent; table 1), followed by a smaller population (14 percent) of light-gray, denser, and more finely crystalline andesite fragments. The color and textural variation between the two components is subtle and quite difficult to discern in clasts smaller than about 5 mm across. Pre-1992 volcanic clasts, some altered to a brick-red color, represent 7 percent of the deposit. Nonvolcanic fragments are a minor component (1 percent). Dry-bulk densities of five samples with median grain sizes of 0.5 to 4.0 mm range from 1.07 to 1.32 g/cm^3. The tan and gray juvenile clasts from the most proximal sample have average densities of 1.76 and 2.27 g/cm^3, respectively (table 2).

Less than 1 percent of the June 27 tephra consists of subangular to subrounded clasts of light-tan, light-gray or white, sugar-textured, and pumiceous (density less than 1.0 g/cm^3) mixtures of feldspar, quartz, scattered mafic minerals and silica-rich glass, here referred to as "silicic pumice" (Nye and others, this volume). These exotics represent entrained basement rock (Miller and others, this volume; Harbin and others, this volume). They are found predominantly on the surface of the June 27 (and subsequent) tephra-fall sequences, which probably reflects their low density and longer residence time in the tephra plume.

AUGUST 18

The main August 18 tephra-fall sequence (fig. 3) consists of a weakly developed, fine-grained basal unit (Layer A'), a moderately well sorted, light-gray to tan, reversely graded unit (layer A) that represents from 60 to 75 percent of the total thickness of any given section, and an upper, well sorted, dark gray, ungraded unit (layer B). Layers A and B are discernible in proximal sections and in thin (less than 2 mm thick) distal tephra deposits as much as 170 km east of Crater Peak.

At three localities 6 to 14 km downwind from Crater Peak, a discontinuous, thin (less than 1–2 mm) dark-gray, medium-grained sand horizon is present beneath layer A. This layer (A') was too thin to sample and was not observed with confidence at all August 18 tephra sections.

Approximately 70 percent of fragments within layer A consists of juvenile, tan, slightly pumiceous, phenocryst-rich clasts. Twenty-three percent of layer A consists of smaller juvenile fragments of andesite that are light to medium gray, microvesicular to dense, and contain sparse lithic inclusions. Clasts that contain both tan and gray components are rare, and in these clasts the boundaries between the tan and gray components are sharp and easily recognized on the basis of color and vesicularity. In addition to the tan and gray clasts, there is a small (approximately 6 percent) population of altered volcanic rock fragments and a small number of white, dense metamorphic clasts. No silicic pumice has been recognized in layer A samples. Dry-bulk densities of five samples range from 0.96 to 1.09 g/cm^3 for layer A. The tan and gray juvenile clasts from layer A have average densities of 1.55 and 2.05 g/cm^3, respectively (table 2).

Most fragments (91 percent) within layer B consist of juvenile, microvesicular to dense, light to medium gray andesite that are similar to the gray fragments of layer A. Tan clasts similar to the dominant component of layer A make up only 6 percent of layer B. Three percent of layer B consists of pre-1992 volcanic clasts and there are only rare fragments of dense, white metamorphic rock. Scattered on the surface of layer B are subangular to subrounded clasts of light-tan to white silicic pumice fragments. Layer B is finer grained at a given distance from the vent than layer A, and it has a dry-bulk density of 1.13 to 1.34 g/cm^3, which is approximately 30 percent higher than that of layer A. Average tan and gray clast densities are 1.50 and 2.01 g/cm^3, respectively (table 2).

In addition to the continuous tephra sequence described above, a prominent ballistic impact zone occurs along the southern margin of the proximal August 18 tephra fall. Extending as much as 10 km from the vent (Waitt and others, this volume), this shower of juvenile and accidental blocks as large as 1 m across occurred primarily late in the eruption, following the main phase of tephra emission (Miller and others, this volume; Waitt and others, this volume).

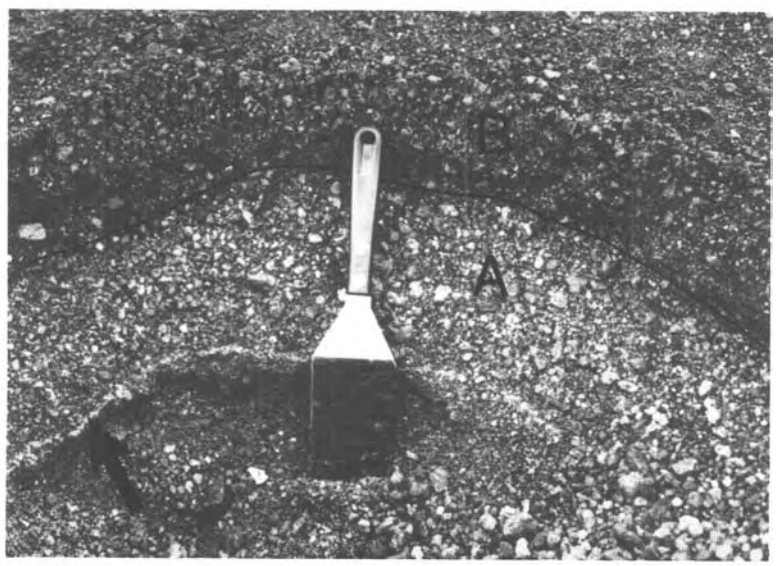

Figure 3. A 16-cm-thick tephra-fall deposit from the August 18, 1992, eruption, located approximately 6.4 km east of Crater Peak, Mount Spurr volcano, Alaska. Layers A and B are labeled. Note reverse grading of layer A. Section rests on sandy tephra from a 1990 eruption of Redoubt Volcano (light horizon; see arrow). Spatula is 23 cm long.

SEPTEMBER 16–17

The September 16–17 fallout deposit contains three layers (layers A', A, and B) similar to those for the August 18 tephra, however the color change that marks the layer A-B transition is not as visually distinct (fig. 4).

At one locality 6.5 km from the vent, a coarse sand unit (layer A') was noted beneath the main sequence. **A** sample of this unit consists of coarse sand-sized, crystal-rich, dense to slightly pumiceous fragments. Both tan and gray colors are represented, estimated visually to be about 60 and 30 percent, respectively. A significant (approximately 10 percent) number of particles are strongly oxidized brick red to purple in color, phenocryst-rich volcanic rock fragments or white to gray crystalline, possibly plutonic or metamorphic fragments.

Layer **A** makes up the lower 70 to 80 percent of the tephrafall, is moderately well sorted, reversely graded, and composed of 79 percent very light tan, slightly pumiceous, phenocryst-rich clasts similar to those in the August 18 tephra. Some of these clasts show a slight yellow tint and are among the most pumiceous of Crater Peak juvenile andesite tephra; a few are highly pumiceous and probably represent the "light-green-gray andesite" (a slight differentiate of the juvenile andesite) of Harbin and others, (this volume). Fifteen percent of layer A consists of smaller fragments of juvenile microvesicular to dense, light- to medium-gray andesite. Pre-1992 volcanic fragments including distinctive rounded clasts of glassy black vesicular rock make up 5 percent of layer A. About 1 percent consists of light-colored plutonic or metamorphic clasts. Dry-bulk densities of two layer A tephra samples are 1.09 and 1.16 g/cm^3. The tan and gray juvenile clasts from layer A have average densities of 1.53 and 2.01 g/cm^3, respectively (table 2).

The September 16–17 layer B is ungraded and finer grained at a given distance from the vent than layer A. Sixty-four percent of the clasts in layer B are light- to medium-gray, microvesicular to dense andesite. Twenty-six percent of layer B clasts are light tan, slightly pumiceous and phenocryst-rich. Dry-bulk densities of two samples are 1.24 and 1.32 g/cm^3, 15 percent greater than layer A. The lower bulk density of September 16–17 layer B compared to August 18 layer B is reflected in the higher percentage of tan clasts in the September 16–17 deposit (table 1). Average clast densities for tan and gray components of layer B are 1.58 and 2.07 g/cm^3, respectively. Pre-1992 volcanic fragments make up nearly 10 percent of layer B. At more distal locations (20 to 30 km from the vent) scattered silicic pumice fragments litter the surface of layer B.

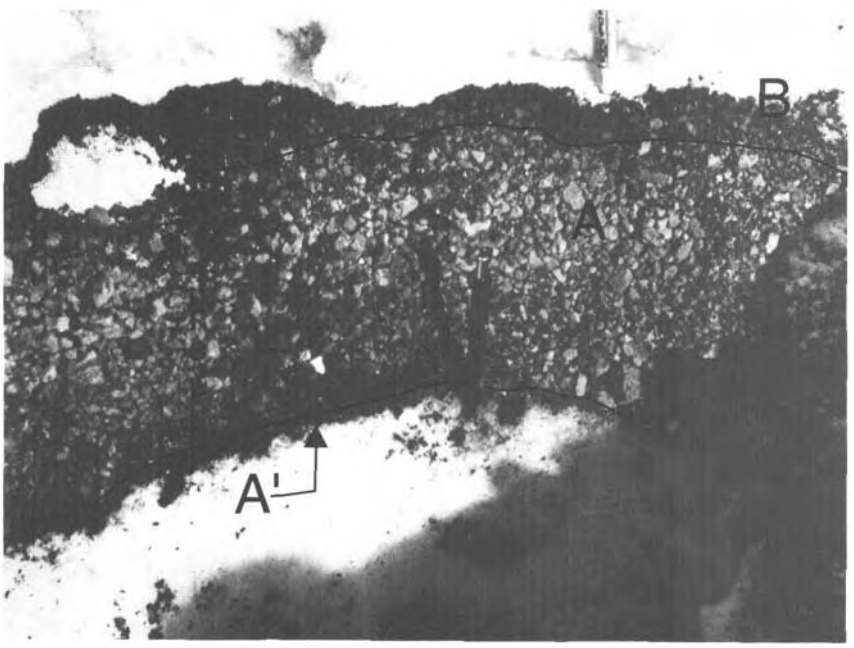

Figure 4. A 17-cm-thick tephra-fall deposit from the September 16–17, 1992, eruption, located approximately 7.2 km northeast of Crater Peak, Mount Spurr volcano, Alaska. Layers A', A, and B are labeled. Note reverse grading of layer A. Section rests on snow. Pencil in center of photograph is approximately 10 cm long.

With increasing distance along the axis of the deposit, the color change in the September 16–17 tephra fall becomes more distinct. About 250 km away, at the northern edge of the deposit, the ash is very light in color, presumably reflecting dominance of the tan juvenile component (layer A?). At the southern margin, the ash is noticeably dark and probably represents the gray juvenile component (layer B?). Given measurable density differences in both dominant clast and bulk densities between layers A and B of 15 to 30 percent (table 2), such asymmetry could reflect within-plume sorting due to slight variations in wind direction with altitude or over the course of the eruption, similar to that documented at Mount St. Helens in 1980 (Sarna-Wojcicki and others, 1981; Waitt and others, 1981).

Ballistic emplacement of coarse breadcrusted bombs consisting principally of tan and gray juvenile components and a smaller lithic component occurred during the September 16–17 eruption. Within approximately 10 km of the vent, along the southern margin of the tephra-fall field, lapilli and bombs were deposited along a narrow corridor. In the snowpack, the ballistic horizon consisted of isolated bombs and lapilli in a matrix of snow and ice that extended down as much as a meter (fig. 5). This disseminated deposit was produced when hot ballistic ejecta impacted snow, differentially melting downward depending on the size of each clast. Melted entry trails were subsequently refrozen to form ice stringers. In part because of the variable settling, there was no time sequence preserved in this ballistic deposit, hence we could not evaluate any stratigraphic information. The collapsed thickness of the deposit after drying ranged from 3 to 4 cm between 6 and 12 km from the vent.

RELATIONS OF TEPHRA-FALL DEPOSITS TO OTHER OBSERVATIONS

To help interpret the proximal tephra-fall record in relation to eruptive processes, the following section summarizes aspects of the timing of tephra fall to pyroclastic flow formation, ballistic ejection of large blocks, and other observations.

JUNE 27

Cloud cover precluded direct observation of the development of the June 27 eruption column or tephra plume. Moreover, strong southerly winds carried the plume northward, 180° away from the path of hot-pyroclast and snow mixtures that swept down the south and southeast flanks of Crater Peak (Meyer and Trabant, this volume). Hence, there is no stratigraphic infor-

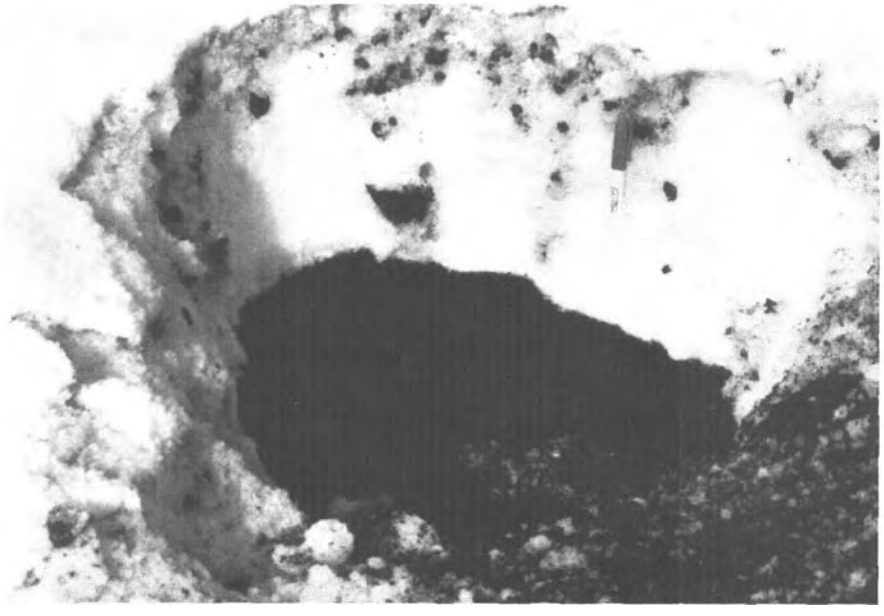

Figure 5. Ballistic tephra-fall deposit from September 16–17, 1992, eruption, located 7 km northeast of Crater Peak, Mount Spurr volcano, Alaska. Projectiles shown here penetrated snow upon impact and left a disseminated horizon of lapilli, bombs, snow, and ice. Dark horizon below is the August 18 tephra section. At the top is a fine ash layer that probably reflects aeolian reworking of material subsequent to the September 16–17 event.

mation to help determine the timing of pyroclastic flow emplacement. Observations inside Crater Peak following the eruption revealed meter-sized bombs littering the surface of a greater than 10-meter-thick deposit of finer grained pyroclastic material interpreted by Miller and others (this volume) as surge deposits. Similarly, numerous coarse juvenile and lithic bombs and associated impact craters dotted the landscape north and east of Crater Peak. Thus, ejection of large bombs, perhaps caused by intermittent phreatomagmatic explosions in the upper part of the conduit, occurred at the end of the June 27 eruption.

Radar images of the June 27 eruption plume are of insufficient quality and pilot reports are too few to establish a good record of the development of the column. However, the maximum radar-discernible column height was recorded 3.3 hours into the eruption (Rose and others, this volume). This is remarkably consistent with RSAM (real-time seismic amplitude measurements; a crude measure of eruption intensity; Murray and Endo, 1989) values, which increased gradually, peaked nearly 3.5 hours into the eruption, and then decreased abruptly during the final hour (fig. 6; McNutt and others, this volume).

AUGUST 18

The opening phase of the August 18 eruption coincided with 12 minutes of tremor recorded on one Spurr seismic station between 3:41 p.m. and 3:52 p.m. ADT (station CRP; McNutt and others, this volume). This event produced a minor tephra plume that, according to pilot reports, had reached approximately 2.5 km above the vent (4.5 km ASL) by 4:20 p.m. ADT. A thin (less than 1 mm), medium sand deposit from this event (layer A') was identified at three localities 4 to 16 km east of the vent. The deposit was not sampled, and the amount of juvenile material vented during this opening phase of eruption is not known.

The main phase of the August 18 eruption occurred from 4:42 p.m. to 8:10 p.m. ADT. Parts of this event were photographed by Paul Palmer on a commercial flight from Anchorage to Iliamna and also by

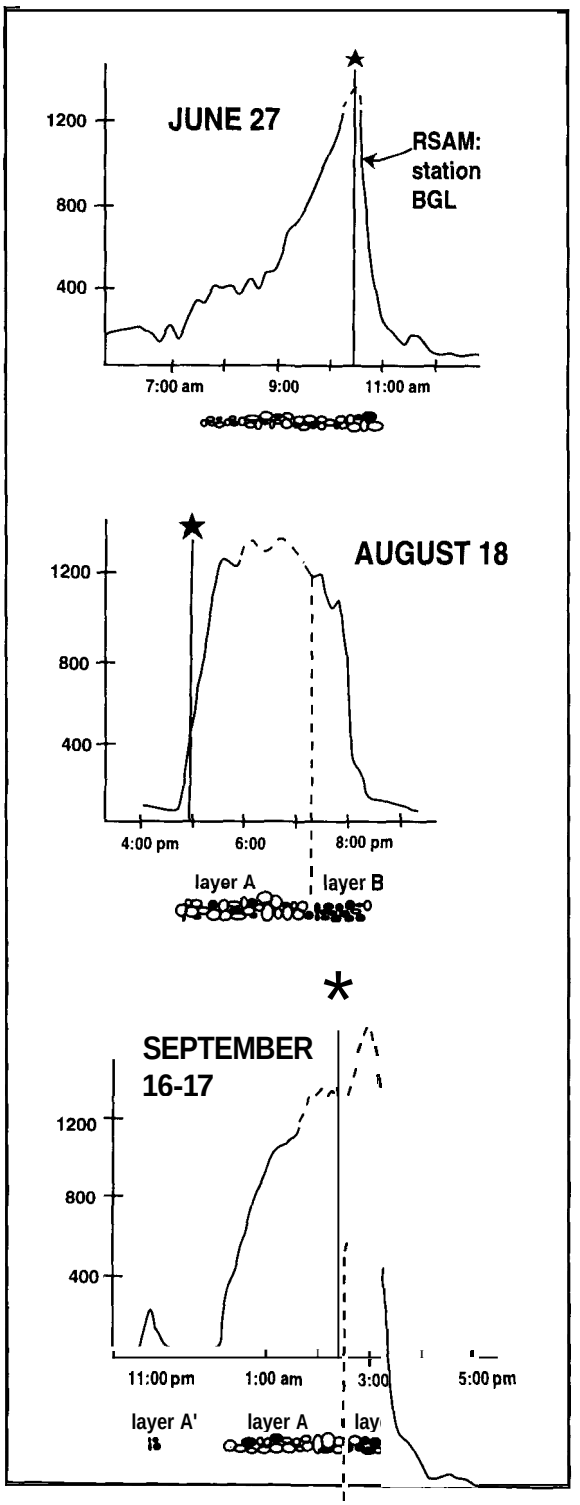

Figure 6. Schematic relation in time between RSAM, maximum eruption column height, tephra production and tephra-fall stratigraphy for the 1992 eruptions of Crater Peak, Mount Spurr volcano, Alaska. Curves are RSAM changes at station BGL, located 7.5 km west of Crater Peak; dashed where values represent instrument saturation and RSAM is unreliable. Vertical axis is digital counts. Stars denote time of maximum column height determined from C-Band radar (Rose and others, this volume). Below each curve is a schematic section of tephra-fall deposit indicating approximate proportion of tan and gray components, changes in grain size and, for August 18 and September 16–17 deposits, position of the layer A–layer B break (long dashes). For September 16–17, sandy layer A' from the opening phase of the eruptions is also shown.

an airborne AVO crew who reached the mountain at about 5:50 p.m. ADT (McGimsey and Dorava, 1994). According to the Palmer photographs, pyroclastic flows, indicated by a light-tan elutriation cloud adjacent to the main eruption column, had already descended the southeast flank by approximately 4:55 p.m. ADT (fig. 7; P. Palmer, oral commun., 1993; Miller and others, this volume). Scaling of photographs indicates an altitude of between 10.5 and 11.5 km ASL for the top of the main eruption plume, consistent with pilot estimates of at least 10 km ASL.

Seismicity indicates that vigorous emission of tephra continued until approximately 8:11 p.m. ADT (McNutt and others, this volume). Intermittent production of pyroclastic flows may have continued throughout the eruption, however the final pyroclastic flows did not extend as far down the flank of Crater Peak. In photographs and from a brief field inspection, these late flows were also darker in color and contained a higher percentage of gray juvenile bombs. Ballistic emplacement of dense bombs, indicated by impact craters on the surface of primary pyroclastic-flow and tephra deposits east of Crater Peak, occurred during the final phase of the eruption (Miller and others, this volume; Waitt and others, this volume).

No complete exposures of the tephra sequence inside Crater Peak were accessible following the August 18 eruption. However, we were able to briefly examine the upper part of the section on the southwest rim of a basin bounded by a tephra rampart (see fig. 1 of Miller and others, this volume). The uppermost unit was a fine, stratified, brown mud approximately 2 to 6 cm thick. This mud overlay an approximately 15-cm-thick sequence of stratified, poorly sorted, brown to black, sandy debris that included a large percentage of oxidized fragments. The lowermost unit was a gravel-boulder horizon, more than several meters thick. It showed strong upward coarsening and many of its angular clasts were highly oxidized. Among the coarsest blocks at the top of this horizon were dense, prismatically jointed, dark-brown juvenile andesite, as much as 50 cm across, and abundant dense, light-colored, aphyric to porphyritic, volcanic bombs as much as 2 m across. This coarse ejecta within the crater is probably correlative with the ballistic field on the southeast flank of Crater Peak (Waitt and others, this volume) and represents a series of closely spaced phreatomagmatic explosions that increased in intensity with time at the very end of the eruption. The sand to silt-sized material capping the entire sequence suggests that low-level phreatic (?) emission of fine material continued after emplacement of ballistics. This may explain the intermittent, low-frequency seismicity in the 24 hours following the eruption, as well as a pilot report of a low (a few hundred meters above Crater Peak) ash and steam column visible above Crater Peak on the morning of August 19.

The radar record of the August 18 eruption is only partially complete, but the maximum recorded height of a radar-discernible plume occurred 13 minutes into the main phase of the eruption (Rose and others, this volume). RSAM amplitude at station BGL reached maximum levels rapidly, and it stayed elevated throughout most of the eruption (fig. 6). Although the record is hampered by saturation problems, RSAM values apparently began to decrease by about 7:50 p.m. ADT, approximately 3 hours into the 3.5-hour eruption (McNutt and others, this volume).

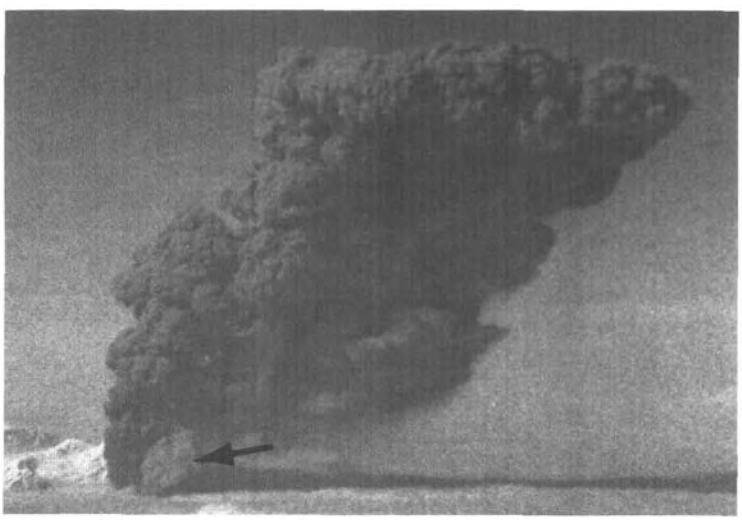

Figure 7. Photograph of the August 18 eruption column and spreading tephra cloud through the window of a commercial flight en route to Iliamna from Anchorage. View direction is approximately north-northwest. The summit of Mount Spurr is just visible to the left of the base of the eruption column. Crater Peak is hidden below a cloud layer, the top of which is about 8,500 feet (2,590 m) ASL. Small, lighter-colored cloud (arrow) is elutriated ash from pyroclastic flows. Time of photograph is approximately 4:55 p.m. ADT, 13 minutes after the onset of the main phase of the eruption. The top of the eruption cloud has reached an altitude of about 11 km ASL. Photograph by Paul Palmer. Used with permission.

SEPTEMBER 16–17

The September 16–17 eruption occurred at night under clear skies. The main phase of the eruption was preceded by an 11-minute burst of seismicity and explosive tephra emission that started at 8:36 p.m. ADT. This eruption was vigorous enough to produce bright flashes on the AVO slow-scan TV camera located at Kasilof, 120 km southeast of Mount Spurr volcano (fig. 1A). In contrast to August 18, this opening phase was detected on C-band radar, hence the tephra column must have extended at least 2 km above Crater Peak (Lee Kelley, NWS, oral commun., 1993). Tephra fall from the first phase was difficult to identify, but at one locality the deposit consisted of a few millimeters of coarse ash and lapilli of both juvenile and accidental material.

The main phase of eruption began just after midnight. Intermittent bursts of incandescence near the base of the eruption column were visible from Anchorage and recorded by the slow-scan camera. Of note is that many of the elongated light flashes captured on film deviate from vertical by several tens of degrees. Miller and others (this volume) relate this directed ejection of incandescent material to the formation of coarse pyroclastic flows on the east flank of Crater Peak. The ballistic field on the southern edge of the September 16–17 tephra deposit may have also formed during episodes of this directed eruption column. Hunters camped 18 km southeast of Crater Peak described incandescent bursts related to projectile impacts into debris on the glaciers east of the cone during the first hours of the eruption; their observations suggest that ballistic ejection occurred over an extended period. Bomb craters on the surfaces of primary pyroclastic-flow and lahar deposits on the glacier east of Crater Peak indicate that ballistic blocks and bombs of appreciable size also fell after generation of pyroclastic flows on September 16–17. There were no bomb craters noted in the lahar deposits that descended the south flank of Crater Peak during the September 16–17 eruption. This observation is consistent with projectiles directed predominantly eastward from the vent, as indicated on the slow-scan images.

Intracrater deposits from the September 16–17 eruption are exposed in a series of scalloped headwalls cut into terraces that ring the inner vent. On the south margin of the crater, approximately the upper meter consists of oxidized, bedded sandy surge deposits capped by fine silt, which was water saturated upon examination a few weeks after the eruption. These sandy surges thicken toward the east sector of the crater where they overlie a massive, poorly sorted very coarse sand to boulder-gravel deposit, the base of which was not exposed.

The C-band radar record of the September 16–17 event is the best of the series and documents a fluctuating tephra column, which finally reached a sustained maximum height of 13.9 km about 2.3 hours into the eruption (Rose and others, this volume). RSAM values at station BGL increased gradually, remained at high levels between about 1:30 a.m. and 3:00 a.m. ADT and decreased abruptly by 3:10 a.m. ADT, about 3 hours into the eruption (fig 6.; McNutt and others, this volume).

DISCUSSION

The presence of tan and gray andesite components in all three eruptions is a primary characteristic of the 1992 Crater Peak tephra. Although petrographically quite similar, the two components differ in density: the tan component is consistently 22 to 24 percent less dense than the gray component (table 2). And, whereas the entire tephra sequence is mixed to some degree for all three eruptions, for August 18 and September 16–17, the tan (less dense) component dominates the lower 60 to 80 percent of the deposits (layer A) and the gray component (more dense) dominates the capping unit (layer B). One explanation of this density stratification is pre-eruption zonation in volatile content. Tan-colored clasts of layer A represent the first material erupted from the upper, volatile enriched part of the magma body; gray-colored clasts represent fragments of melt stored slightly deeper and depleted, relatively, in volatiles. The imperfect separation of components (mixing of tan and gray within layers A and B) may reflect nonuniform withdrawal of magma from the conduit (Blake and Ivey, 1986).

If the layer A-B divisions within the August 18 and September 16–17 deposits reflect a change in magmatic volatile content, a coincident and measurable change in the behavior of the eruption column might be expected. To test this, we superimposed a schematic representation of the fallout record on plots of RSAM, the only independent instrumental measure of eruption intensity available for the entire eruption series (fig. 6). To construct figure 6, seismicity, pilot reports, radar data, the few eyewitness observations, and slow-scan video were used to roughly constrain the period of tephra production. Note that we have assumed by the superposition of the RSAM record over the schematic tephra-fall section that there is an instantaneous relation between seismicity and tephra accumulation; in reality, there must be some delay.

For the June 27 eruption, there is no break in tephra-fall stratigraphy where the proportions of tan to gray components change. Hence, based solely on field observations and the samples in hand, we can-

not simply relate the RSAM curve to the proportion of clast type. For the August 18 eruption, radar data (Rose and others, this volume) and pilot reports allow fairly accurate limits to be placed on the timing of tephra production. In figure 6, the layer A-B transition was placed approximately 65 to 70 percent through the eruption on the basis of field measurements of relative thicknesses. Projecting this break onto the RSAM curve suggests that the later stage of tephra production (dominated by the gray component of layer B) was associated in time with a period of declining RSAM. This association could be explained by tapping of a deeper, more degassed part of the magma body, which resulted in lower eruption column vigor. Unfortunately, radar data are lacking for the later stages of the eruption and we cannot independently evaluate column height. For the September 16–17 eruption, the layer A-B transition occurs during a period of instrument saturation, hence it is difficult to assess the relation of stratigraphy to RSAM data for station BGL. To summarize, only data for the August 18 eruption suggest a possible correlation between eruption intensity and clast type erupted.

Another prominent characteristic of the August 18 and September 16–17 layer A deposits, and to a lesser extent the June 27 deposits, is reverse grading. Reverse grading in tephra-fall deposits can reflect a decrease in the angle of pyroclast ejection, changes in wind velocity, or increasing magma discharge over the course of an eruption. For both the August 18 and September 16–17 eruptions, photography and slow-scan TV images do not support any progressive changes in the inclination of the eruption column. Furthermore, the narrow fallout patterns indicate that local winds were steady in speed and direction over the course of all three events. Thus, we propose that the reverse grading in the June 27 and lower August 18 and September 16–17 deposits is a result of an increase in magma discharge at the vent.

To test this, we compared the stratigraphic position of maximum clast size within the resulting deposits and the times of maximum plume heights and RSAM peaks (fig. 6). For June 27, there is a good correlation among all three parameters. For August 18 layer A, maximum grain size is approximately coincident with the RSAM peak (although saturation makes this uncertain). More importantly, the amplitude of volcanic tremor recorded at more distant stations reached a maximum about halfway through the August 18 eruption (S. McNutt, written commun., 1993). Similarly, the maximum clast size is present very near the middle of the deposit. Maximum plume height on August 18, however, occurred only minutes after the onset of the eruption. For September 16–17 layer A, maximum clast size and maximum plume height are approximately congruent. While the RSAM data for September 16–17 are difficult to interpret, the strongest tremor occurred during the middle of the eruption (S. McNutt, written commun., 1993). Thus, grain size maximums for all three eruptions occur at stratigraphic positions that approximately mirror the times of maximum seismicity (as measured by a combination of RSAM and tremor amplitude). The large offset in time of maximum plume height for the August 18 eruption and the maximum clast size in the resulting tephra-fall deposit remains an enigma and may be an artifact of poor radar sampling (Rose and others, this volume). A more careful analysis of changes in grain size and clast characteristics with stratigraphic height for all three deposits is needed to determine the exact mechanism behind the development of reverse grading.

In other stratigraphic studies of tephra-fall deposits, color and clast-size changes are associated with small but measurable chemical or mineralogic variations, interpreted to reflect pre-eruption chemical zonation in the magma chamber (Bursik and others, 1992; Criswell, 1987; Carey and Sigurdsson, 1987). Whole-rock major- and trace-element analyses of individual tan and gray clasts for Crater Peak, however, show no significant differences between the two clast types either within or through the eruption series.

Major- and trace-element chemical data for tephra normalized to average 1992 andesite blocks retrieved from pyroclastic-flow deposits are shown in figure 8. Tan tephra are nearly identical to the andesite with the possible exception of low Cs and Rb concentrations in two samples. But even these are less than 25 percent different from the andesite values (0.1 ppm Cs and 3 ppm Rb), and they are nearly within two standard deviations of the andesite mean. Over half of the gray tephra samples analyzed to date have concentrations of all elements similar to the andesite blocks. However, some gray tephra samples are more heterogeneous. These samples are highly enriched in Cs (as much as 3.7 times the andesite mean) and also enriched in Sc, Cr, and Ni. The paired enrichment in alkalies and compatible transition metals suggests contamination by metamorphic country-rock represented by partially melted xenoliths found in the 1992 pyroclastic-flow deposits (see Nye and others, this volume). However, simple xenolith contamination is not controlling the high Cs in these samples (fig. 9). Those samples with very high Cs do not have the low CaO or high Th that xenolith-contaminated samples would have.

Processes controlling the chemistry of the gray tephra samples are not clearly known but may include accumulation of mafic phenocrysts, vapor-phase transport of some metals, or incorporation of highly fractionated material from the margin of a sub-Crater Peak

magma chamber. This final possibility is supported to some extent by the recovery of rare, light gray, moderately siliceous pumice lapilli from the June 27 eruption, which are similar to the divergent tephra samples in Cs, Ca, Th, U and, to a lesser extent, Cr and Ni (Nye and others, this volume).

Finally, the gray tephra samples that are chemically unlike the andesite have compositions governed by chemical heterogeneities on a very small scale (about 10 g of material). Only when small sample amounts were analyzed were heterogeneities found, and the magnitude of those heterogeneities varied between splits. When larger samples (greater than 50 g) were processed, the tephra analyses were generally closer to that of the andesite. In summary, both tan and gray tephra are chemically similar or identical to the 1992 andesite and to each other. Differences that can be found are slight and related to contamination by poorly understood components on a very localized scale.

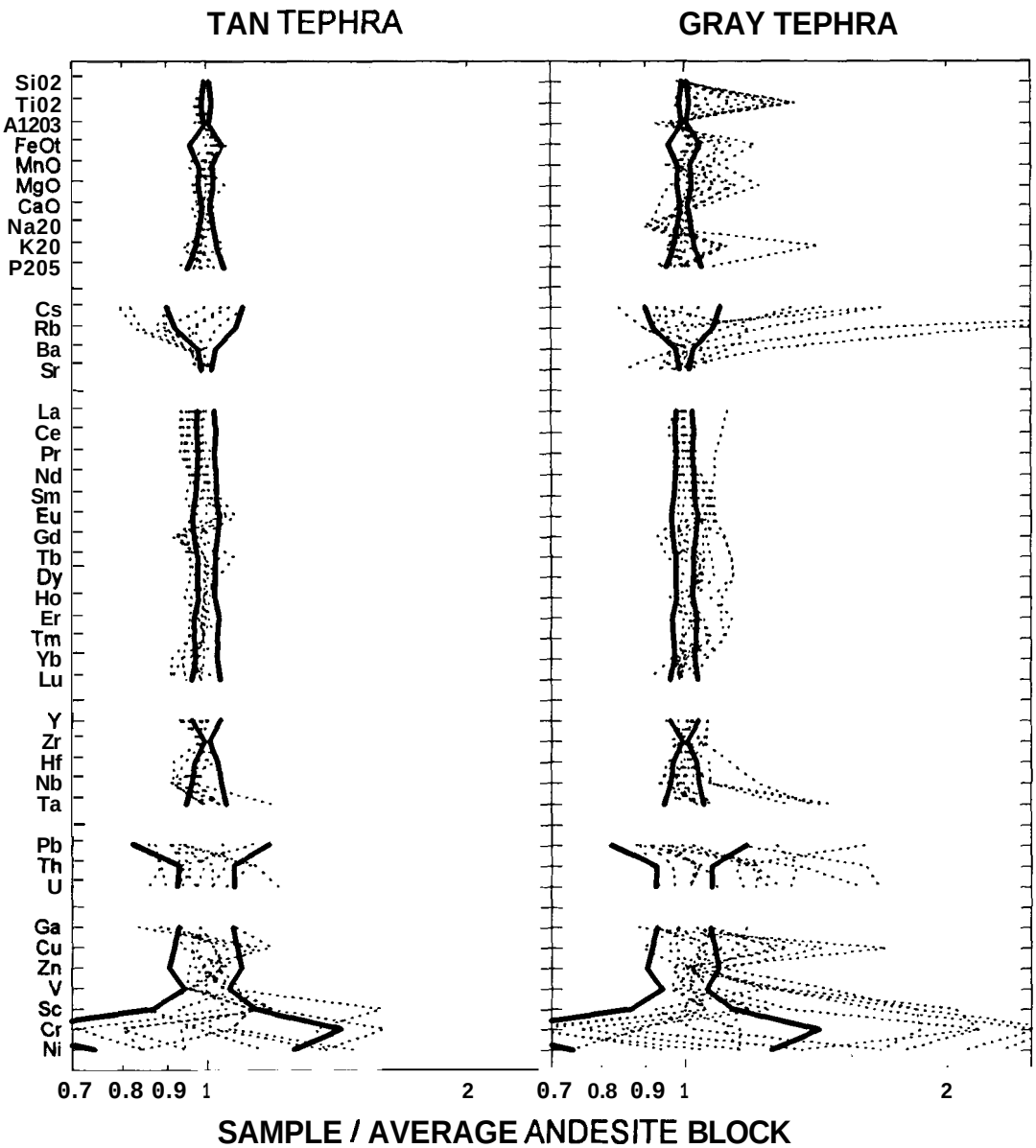

Figure 8. Whole-rock major- and trace-element compositions of selected tan and gray tephra lapilli from the 1992 eruptions of Crater Peak, Mount Spurr volcano, Alaska. FeO_t = FeO total. Dark lines represent one standard variation about the mean of 18 juvenile andesite blocks from all phases of each eruption (see Nye and others, this volume).

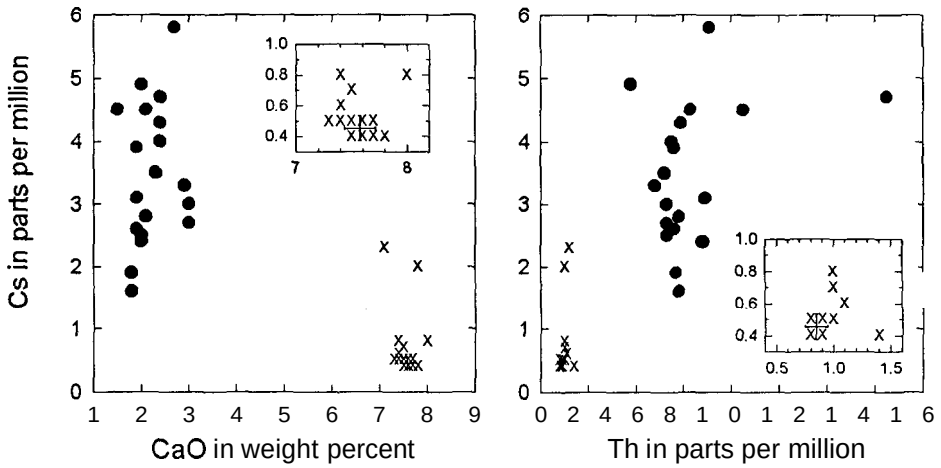

Figure 9. Variations of CaO and Th with Cs. Filled circles, analyses of partially melted aluminous metamorphic xenoliths ejected during the 1992 eruptions of Crater Peak, Mount Spurr volcano, Alaska (see Nye and others, this volume); X, tan and gray tephra analyses of fig. 8; and +, average analysis of the 1992 juvenile andesite blocks (+ spans one standard deviation about the mean of 18 samples). Note that the majority of tephra are similar to the andesite and that those dissimilar from the andesite do not form mixing arrays with the xenoliths.

SUMMARY

Three vulcanian to subplinian eruptions of Crater Peak at Mount Spurr volcano during 1992 produced tephra-fall deposits that extend north, northeast, and east of the volcano. The eruptions were similar in magnitude, style, and duration and produced, respectively, 44, 52, and 56 x 106 m^3 of bulk tephra (12, 14, and 15 x 106 m3 DRE) in 3.5 to 4.0 hours of vigorous eruption. Measured thicknesses ranged from about 1 m at the base of the vent to less than 1 mm at a distance of 200 km from Crater Peak.

Fallout tephra from the 1992 eruptions of Crater Peak consists predominantly of two texturally distinct but chemically similar juvenile andesitic components. Density data suggest that prior to each eruption, a physically zoned magma body existed beneath Crater Peak. The zonation is best explained by upward migration of volatiles and formation of a gas-charged upper part of the chamber. The presence of both components in all three eruptions suggests that such zonation can develop rapidly (that is, within 4 to 6 weeks, the time intervals between eruptions). Alternatively, each eruption may have tapped only a part of an initially zoned chamber emplaced prior to the first eruption on June 27. Minor settling of mafic phenocrysts, contamination of juvenile andesite by remelted country rock, incorporation of a highly fractionated derivative of the juvenile andesite, and vapor-phase transport of some elements may account for observed small geochemical variations of individual tephra clasts.

Future analytical work on the Crater Peak tephra-fall deposits will focus on clarifying the extent and nature of small-scale geochemical heterogeneities; quantifying vesicularity, phenocryst, and groundmass textures to address the root cause of the systematic density differences (Gardner and others, 1993); and examining clast grading and density characteristics in more detail to reconstruct changes in eruption-column energetics through each event.

REFERENCES CITED

Alaska Volcano Observatory, 1993, Mt. Spurr's 1992 eruptions: Eos, Transactions of the American Geophysical Union, v. 74, no. 19, p. 217–222.

Blake, S.R., and Ivey, G.N., 1986, Magma mixing and the dynamics of withdrawal from stratified reservoirs: Journal of Volcanology and Geothermal Research, v. 27, p. 153–178.

Brantley, S.R., ed., 1990, The eruption of Redoubt Volcano, Alaska, December 14,1989 – August 31,1990: U.S. Geological Survey Circular 1061, 33 p.

Bursik, M.I., Sparks, R.S.J., Gilbert, J.S., and Carey, S.N., 1992, Sedimentation of tephra by volcanic plumes: I. Theory and its comparison with a study of Fogo A plinian deposit, Sao Miguel (Azores): Bulletin of Volcanology, v. 54, p. 329–344.

Carey, S., and Sigurdsson, H., 1987, Temporal variations in column height and magma discharge rate during the 79 A.D. eruption of Vesuvius: Geological Society of America Bulletin, v. 99, p. 303–314.

Criswell, C.W., 1987, Chronology and pyroclastic stratigraphy of the May 18, 1980 eruption of Mount St. Helens, Washing-

ton: Journal of Geophysical Research, v. 92, p. 10,237 – 10,266.

Fierstein, J., and Nathenson, M., 1992, Another look at the calculation of fallout tephra volumes: Bulletin of Volcanology, v. 54, p. 156–167.

Gardner, C.A., Neal, C.A., and McGimsey, R.G., 1993, Volatile zonation in the Crater Peak magma: Evidence from the 1992 tephra-fall deposits [abs.]: Eos, Transactions of the American Geophysical Union, v. 74., no. 43, p. 621.

Hoblitt, R.P., and Harmon, R.S., 1993, Bimodal density distribution of cryptodome dacite from the 1980 eruption of Mount St. Helens, Washington: Bulletin of Volcanology, v. 55, no. 6, p. 421437.

McGimsey, R.G., and Dorava, J., 1994, Video of the August 18, 1992, eruption of Crater Peak vent on Spurr volcano, Alaska: U.S. Geological Survey Open-File Report 94-614.

Murray, T.L., Bauer, C.I., and Paskievitch, J.F., 1994, Using a personal computer to obtain predicted plume trajectories during the 1989-90 eruption of Redoubt Volcano, Alaska: Casadevall, T.J., ed., *in* U.S. Geological Survey Bulletin 2047, p. 253–256.

Murray, T.L., and Endo, E.T., 1989, A real-time seismic amplitude measurement system (RSAM): U.S. Geological Survey Open-File Report 89-684, 21 p.

Sarna-Wojcicki, A.M., Shipley, S., Waitt, R.B., Jr., Dzurisin, D., and Wood, S.H., 1981, Aerial distribution, thickness, mass, volume, and grain size of air-fall ash from the six major eruptions of 1980: U.S. Geological Survey Professional Paper 1250, p. 577–600.

Scott, W.E., and McGimsey, R.G., 1994, Character, mass, distribution, and origin of tephra-fall deposits of the 1989–90 eruption of Redoubt Volcano, south-central Alaska: Journal of Volcanology and Geothermal Research, v. 62, p. 251–272.

Till, A.B., Yount, M.E., Riehle, J.R., 1993, Redoubt Volcano, Cook Inlet, Alaska: A hazard assessment based on eruptive activity since 1968: U.S. Geological Survey Bulletin 1966, 19 p.

Waitt, R.B., Jr., Hansen, V.L., Sarna-Wojcicki, A.M., and Wood, S.H., 1981, Proximal air-fall deposits of eruptions between May 24 and August 7, 1980 - stratigraphy and field sedimentology: U.S. Geological Survey Professional Paper 1250, p. 617–628.

Wilcox, R.E., 1959, Some effects of recent volcanic ash falls with special reference to Alaska: U.S. Geological Survey Bulletin 1028, p. 409476.